

Strain mediated adatom stripe morphologies on Cu<111> simulated.

Wolfgang Kappus
wolfgang.kappus@t-online.de

v02: 2013-01-29

Abstract

Substrate strain mediated adatom configurations on Cu<111> surfaces have been simulated in a coverage range up to nearly 1 monolayer. Interacting adatoms occupy positions on a triangular lattice in two dimensions. The elastic interaction is taken from earlier calculations, short range effects are added for comparison. Dependent on the coverage different morphologies are observed: Superlattices of single adatoms in the 0.04 ML region, ordered adatom clusters in the 0.1 ML region, elongated islands in the 0.3 ML region, and interwoven stripes in the 0.5 ML region. In the region above the sequence is reversed with occupied and empty positions complemented. Stronger short range interactions increase the feature size of the clusters and reduce their lattice order. The influence of the substrate elastic anisotropy turns out to be significant. Results are compared with morphologies observed on Cu<111> surfaces and the applicability of the model is discussed.

1. Introduction

Regular self-assembled adatom structures, ranging from superlattices via nanodot arrays to strain relief pattern are interesting for various general and technological reasons, reviews were given in [1,2]. While interactions of adatoms comprise various mechanisms [3] the focus on elastic interactions in this paper is driven by the question on their importance compared with other interactions. In recent calculations on the stability and dynamics of strain mediated superlattices it was shown that the role of elastic interactions was underestimated compared with surface state mediated interactions [4], so other surface phenomena seem worth to be discussed in the light of strain mediated interactions. Anisotropies of adatom pattern can act as a probe for indicating strain mediated interactions via correlation to anisotropies of the substrate elastic constants.

The calculations on the stability and dynamics of strain mediated superlattices [4] covered a low coverage region and left the question open how adatoms

arrange under equilibrium conditions when the coverage is increased. The experiments of Plass et al. on domain patterns [5] provide a challenge to prove the ability of an elastic continuum theory in building a bridge between superlattices and stress relief patterns. Such bridge was built before with a Green function method for the non-equilibrium case [6].

The focus on Cu<111> has good reasons as well: Cu is among the substrates with the highest elastic anisotropies and Cu<111> seems to be a preferred surface for experiments. Unfortunately the crystal directions are often not published, so a solid proof of elastic effects is hindered. The predictions of this work are intended to allow a verification of the theory by experiments.

The model used in this work to simulate adatom morphologies is an adaptation of the one used in [4]. The latter used a grid-less molecular dynamic algorithm suited for low coverages. For the higher coverages up to 1 ML and the <111> surface discussed in this work it had to be converted to a grid base where adatom positions reside on a triangular lattice representing identical threefold coordinated substrate sites. The interaction mechanism has been kept; it is based on the isotropic stress individual adatoms on threefold coordinated sites exert to their neighborhood. The limitations of such interaction mechanisms and of other model assumptions are discussed below.

The model results will be presented as sample adatom configurations for increasing coverages and for three variants of the interaction. The variants stand for three different strengths of short range interactions and should give an idea of the interplay between short- and medium-term interactions. The model results will also be presented as pair distributions derived from averaging over sample configurations.

This work is organized as follows: In section 2 the details of the interaction model are recalled and the simulation model is detailed. Furthermore the calculation method for pair distributions is described. In section 3 the model results will be presented as sample adatom configurations and as pair distributions derived from averaging over sample configurations. For symmetry reasons the pair distributions will cover 30° segments only. In section 4 the model assumptions are reviewed, the model results are summarized and compared with a few experiments and open questions are addressed. Section 5 closes with a summary of the results.

2. Model details

In this section the elastic interactions used within the model are recalled, the grid based algorithm for the Molecular Dynamic simulations is introduced and the method for deriving adatom pair distributions is explained. Also scaling relations, intended for the interpretation of experiments, are recalled.

2.1. Elastic interactions of adatoms

Following [8] the interaction of adatoms located at the origin and at \vec{s} using polar coordinates (s, ϕ) for their distance $s = |\vec{s}|$ and pair direction angle ϕ with respect to the crystal axes is given by

$$U(s, \phi) = (2\pi)^{-1} \sum_p \omega_p \frac{\cos(p\phi) \cos(p\frac{\pi}{2}) \Gamma(\frac{p+3}{2}) s^p {}_1F_1\left(\frac{p+3}{2}; p+1; \frac{-s^2}{4\alpha^2}\right)}{2^{p+1} \Gamma(p+1) \alpha^{p+3}}, \quad (2.1)$$

where ${}_1F_1$ denotes the Hypergeometric Function, $\Gamma(p)$ the Gamma function, $\alpha = \sqrt{2}/2$ is a cutoff length defining height and location of the potential wall and the medium range potential, and the ω_p denote coefficients of a cosine series describing the solution of an elastic eigenvalue problem [8]. The dominating isotropic $p=0$ term of Eq. (2.3) is negative for small s describing a potential well (i.e. an attractive potential), has a positive wall (i.e. a repulsive potential) at $s=s_w$ and approaches infinity with a s^{-3} law. For elastic anisotropic substrates like Cu the $p>0$ terms describe the anisotropic part of the interaction and influence the height of the positive wall in dependence of the pair direction angle ϕ with respect to the crystal axes. Tab. 1 shows the ω_p for the elastic adatom interaction on Cu<111> and W<111> (for comparison) calculated as outlined in [8]. We note the units of the ω_p :

- the numerator is P^2 , the square of a scalar parameter P describing the lateral stress magnitude an adatom exerts to the surface

- the denominator is the c_{44} elastic constant of the substrate.

For details of the parameter P see [8].

Substrate	c_{11}	c_{12}	c_{44}	ζ	ω_0	ω_6	ω_{12}
Cu	169.	122.	75.3	-1.376	-1.01	-0.007	+0.0004
W	523.	203.	160.	0.	-0.720	0.	0.

Table 1. Substrate Elastic Constants c_{ik} (GPa) from [9], anisotropy $\zeta = (c_{11} - c_{12} - 2c_{44})/c_{44}$ and coefficients ω_p (in P^2/c_{44} units) on Cu <111> and W<111>

In the present analysis the strong attractive interaction of Eq. (2.1) in the region $s < s_w$ is replaced by three variants to study the influence of short range interactions - in addition to the elastic interaction - on the medium range adatom morphology:

- variant 1 as used and described in [4]

$$U_1(s, \phi) = U_w + U_{wp} \cos(p\phi) \frac{s}{s_w} \text{ for } s < s_w, \quad (2.2)$$

where U_w describes the wall height, U_{wp} the wall anisotropy variance, and s_w is the location of the wall maximum,

- variant 2, describing additional attraction between next neighbors

$$U_2(s, \phi) = 0 \text{ for } s < s_0, \quad (2.3)$$

where s_0 is defined by $U(s_0, \phi) = 0$, covering the range $s \lesssim 1.75$, significantly smaller than s_w ,

- variant 3, describing stronger attraction between next neighbors

$$U_3(s, \phi) = -5 k_B T \text{ for } s \leq s_3, \quad (2.4)$$

where s_3 is the next neighbor distance. The value -5 is chosen to get an equidistant series of U values.

2.2. Simulations

The Molecular Dynamics grid-less algorithm used in [4] turned out unstable and inefficient in the coverage range $\theta > 0.1$. Therefore a triangular grid algorithm has been used instead. The triangular grid represents adatom positions on a $\langle 111 \rangle$ surface with threefold symmetry fulfilling the symmetry condition used for the adatom generated surface stress [8]. Periodic boundary conditions were applied to avoid the problem of adatom diffusion to the boundary. The hexagon diameter of 48 units was chosen to keep the computing time in the range of hours while the interaction $u(s=24)$ has decreased well below 0.01. Temperature effects are treated by the normalized interaction

$$u(s, \phi) = U(s, \phi) / k_B T. \quad (2.5)$$

Not knowing the size of the stress parameter P and as in [4] the average wall height is assumed $u_W=5$ and this choice determines all $u(s, \phi)$.

In our grid algorithm an adatom configuration is described by a set of occupation numbers $\{\tau_i\}$, $\tau_i \in \{0, 1\}$. Starting from a random k member adatom configuration $\{\tau_{i,0}\}$, step $n + 1$ $\{\tau_{i,n+1}\}$ evolves from step n $\{\tau_{i,n}\}$ by comparing the total interaction of each adatom i

$$u_{\text{tot}}(i) = \sum_{j=1}^k u_{ij} \tau_j \quad (2.6)$$

with that of its empty next neighbor positions. If a next neighbor position m has less total interaction, the adatom i jumps to that position m. So adatoms move around under the force field of all neighbors until all interaction is minimized.

The iterations are terminated when either no more jumps occur or when loops of identical configurations are detected.

2.3. Pair distribution

The adatom pair distribution g_{ik} is calculated by averaging occupation pairs

$$g_{ik} = \langle \tau_i \tau_k \rangle / \theta^2, \quad (2.7)$$

where θ denotes the coverage. So $g_{ik}=1$ in a random configuration, $g_{ik}>1$ if the pair $\{\tau_i, \tau_k\}$ occurs more likely and $g_{ik}<1$ if the pair $\{\tau_i, \tau_k\}$ occurs less likely. It is the discrete variant of $g(s, \theta)$ calculated in [7] with a 2-dimensional Born-Green-Ivon type integral equation.

2.4. Pair distribution scaling

For the discussion of experimental results in section 4.5 we will need to recall scaling properties of the continuous pair distribution $g(s, \theta)$ as outlined in [7]. In the long range isotropic limit the adatom-adatom interaction becomes

$$u(s) = u_0 s^{-3} + O(s^{-5}), \quad s \gg s_0 \quad (2.8)$$

and the pair distribution scales

$$g(s, u_0, \theta) = g(\tau s, \tau^3 u_0, \tau^{-2} \theta) \quad (2.9)$$

with a scaling factor τ . In other words the pair distribution has the same shape if simultaneously the length is doubled, the interaction is eightfold and the coverage is reduced by a factor of four. We also note from Eq. (2.5) an eightfold normalized interaction u results if the interaction U is kept constant and the temperature T is reduced by a factor of eight. We further note that doubling the stress parameter P increases the interaction U by a factor 4.

3. Results

The results are presented in pairs of figures, the first of which shows a sample adatom configuration in a hexagon area simulated according to section 2.2 and the second shows an equivalent pair distribution g_{ik} according to section 2.3 and averaged over configuration samples. The presentation comprises varying coverages θ and interactions U_i (sections 3.3 to 3.5) to study the influence of short range interactions. We note the different notation of interactions U_i and scaled interactions u_i according to Eq. (2.5).

The adatom pair distributions are shown as dots at lattice positions in a 30 degree sector for symmetry reasons. A color code with different colors/ darkness is used to mark pair distribution ranges:

- $g_{ik} \geq 1.5$ black
- $1.5 > g_{ik} \geq 1.0$ blue/ dark gray
- $1.0 > g_{ik} \geq 0.5$ green/ medium gray
- $g_{ik} > 0.5$ yellow/ light gray
- $g_{ik} \leq 0.5$ white.

Since the algorithm used is different from the one previously used [4] the results section starts with a reference. Unfortunately a fault in the code of [4] was just detected: the $\cos(p\pi/2)$ term in Eq. (2.1) was omitted and therefore the results in [4] were rotated 30° compared to the current corrected version.

3.1. Reference configuration

Fig. 2.a shows empty (yellow points) and occupied positions (red points) of a triangular lattice. The interaction used is U_1 and described by Eqs. (2.1) and (2.2). Fig. 1.a acts as reference to [4] with a coverage $\theta=0.045$ to demonstrate that the new algorithm leads to the same sample results except a 30° rotation (as stated before). A substrate aligned superlattice of adatoms and a few dimers with a lattice parameter of 5 grid units shows up like in the reference.

Fig. 1.b. shows the adatom pair distribution in a 30 degree sector taken from a configuration average. Black points near $s_{\langle 1-21 \rangle}=3*\sqrt{3}$ and $6*\sqrt{3}$ lattice spacings and at $s_{\langle 1-10 \rangle}=9$ reflect the (not quite perfect) aligned monomer superlattice. We note a blue dot at $1 s_{\langle 1-10 \rangle}=1$ reflecting a small population of next neighbor sites.

3.2. Influence of substrate elastic (an-)isotropy

Previous investigations showed a strong influence of the substrate elastic constants on the adatom pair distribution [7]. A triangular grid algorithm could compromise such delicate matter. To prove the grid algorithm properly handling substrate isotropy, the elastic constants of tungsten were used as reference (see Tab.1). Fig.2 shows the resulting pair distribution for a coverage $\theta=0.045$ in a 30 degree sector. It shows (irrespective statistical variances) the characteristic rings at 5, 10, 15 substrate lattice spacings already discussed in [7].

Isotropy could also be compromised by adatom multiples. Though there are almost no angular moments of circular clusters in the relevant distance of 5 lattice constants, adatom straight tripoles would generate differences in the interaction of up to 18% (less repulsive orthogonal to the axes).

3.3. Adatom configurations for coverages between 0.1 and 1 monolayer

To stay consistent with [4] we will use in this section the short range interaction $U_1(s, \phi)$, Eq. (2.2) and thus the more repulsive variant 1. In 0.2 steps the coverage is increased in Figs. 3.a. to 3.h showing the effects of a subsequent population of the 2-dimensional triangular lattice up to 0.9 monolayers and the corresponding pair distributions according to Eq. (2.7).

Fig.3.a shows a sample configuration at coverage $\theta=0.1$ and Fig.3.b shows the equivalent pair distribution taken from a configuration average. The black dots in Fig.3.b near $s_{\langle 1-21 \rangle}=3*\sqrt{3}$ and at $s_{\langle 1-10 \rangle}=8$ reflect a superlattice with a superlattice constant of nearly 5 substrate lattice spacings consisting of monomers, dimers, trimers and a few 4-mers. The dark dot at $s_{\langle 1-10 \rangle}=1$ reflects the high amount of next neighbors.

Fig.3.c shows a sample configuration at coverage $\theta=0.3$ and Fig.3.d shows the equivalent pair distribution taken from a configuration average. The black dot in Fig.3.d near $s_{\langle 1-21 \rangle}=3*\sqrt{3}$ again reflects a superlattice with a superlattice constant of nearly 5 substrate lattice spacings consisting of circular and

elongated n-mers. A few thin bridges between islands should be noted in Fig.3.a.

Fig.3.e shows a sample configuration at coverage $\theta=0.5$. Elongated islands have now merged to an interwoven stripe structure. Fig.3.f shows the equivalent pair distribution taken from a configuration average. The pair distribution indicates a characteristic distance of 4 to 5 substrate lattice spacings. g_{ik} values of 1.0 at $s_{\langle 1-10 \rangle}=5$ to 6 and of 1.2 at $s_{\langle 1-21 \rangle}=3*\sqrt{3}$ indicate a weak stripe alignment towards $\langle 1-21 \rangle$. We note in Fig.3.e. a similar vacancy stripe structure.

Fig.3.g shows a sample configuration at coverage $\theta=0.9$. The vacancies are forming aligned dimers, trimers, n-mers like the adatoms in Fig.3.a.

Omitting intermediate results for coverages $\theta > 0.5$ has a good reason: they show vacancy structures inverse to adatom structures at $(1-\theta)$. Therefore a vacancy pair distribution

$$g_{ik}^{\text{vac}} = \langle (1 - \tau_i)(1 - \tau_k) \rangle / (1 - \rho)^2, \quad (3.1)$$

is introduced. g_{ik}^{vac} measures the likeliness of vacancy pairs $\{(1-\tau_i), (1-\tau_k)\}$.

Fig.3.h shows the vacancy pair distribution taken from a configuration average at coverage $\theta=0.9$. It shows almost the same structure as the adatom pair distribution at coverage $\theta=0.1$ in Fig.3.b, indicating a superlattice now of vacancy monomers, dimers, trimers and some 4-mers.

In summary the interaction u_1 with increasing coverage leads to clusters growing on superlattice positions from mono- to n-mers. Subsequently elongated islands are formed, merge to stripes at 0.5 ML and then the sequence is reversed with empty positions instead of occupied ones. Such changes in adatom morphology are summarized in Tab.2.

Coverage	Form	Superlattice	Inversion	Adatoms	Vacancies	FeatureSize
				avg.	avg.	avg.
0.045	monomers	Y		1		5
0.1	dimers	Y		2		4.8
0.3	triangles/linear	Y		7		4.8
0.5	coherentstripes					4.6
0.9	dimers	Y	Y		2	

Table 2. Changes of adatom morphology with increasing coverage, simulated with interaction u_1

3.4. Influence of short range interactions, the U_2 example

Variant 1 $U_1(s, \phi)$, Eq. (2.2) of the short range interaction was used in [4] to enable convergence of the BGY type integral equation. Compared with Eq. (2.1) it describes an effective repulsive interaction in the short range. To show the

influence of short range interactions, variant 2 $U_2(s, \phi)$, Eq. (2.3) is chosen less repulsive and therefore promotes adatoms to nucleate at next neighbor sites. We note in the pair distributions below black or dark dots at next neighbor distance.

Fig.4.a shows a sample configuration with short range interaction $U_2(s, \phi)$, Eq. (2.3) at coverage $\theta=0.1$. The superlattice consists of many n-mers and some smaller aggregates. Fig.4.b shows the equivalent pair distribution taken from a configuration average. The black dots at $s_{\langle 1-21 \rangle} = 3\sqrt{3}$ indicate a superlattice with a lattice constant of slightly above 5. The blue dots at a distance of about 10.5 in all directions indicate a trend towards isotropy, i.e. a reduced superlattice order compared to Fig. 3.b.

Fig.4.c shows a sample configuration with short range interaction $U_2(s, \phi)$, Eq. (2.3) at coverage $\theta=0.3$. The superlattice consists of islands some of which have merged to elongated islands. Small bridges between islands create dog-bone-like shapes. Fig.4.d shows the equivalent pair distribution taken from a configuration average. The blue dots indicate an isotropic ring structure with a characteristic distance of nearly 6, the g_{ik} values of 1.2 at $s_{\langle 1-10 \rangle} = 5$ and of 1.35 at $s_{\langle 1-21 \rangle} = 3\sqrt{3}$, however, indicate a weak island alignment towards $\langle 1-21 \rangle$.

Fig.4.e shows a sample configuration with short range interaction $U_2(s, \phi)$, Eq. (2.3) at coverage $\theta=0.5$. The islands of lower coverages have now merged to an interwoven but incoherent stripe structure with an average stripe broadness of nearly 3. Fig.4.f shows the equivalent pair distribution taken from a configuration average. The blue dots again pretend an isotropic ring structure with a characteristic distance of 6, the g_{ik} values of 1.1 at $s_{\langle 1-10 \rangle} = 5$ to 6 and of 1.2 at $s_{\langle 1-21 \rangle} = 3\sqrt{3}$, however, indicate a weak stripe alignment towards $\langle 1-21 \rangle$. Compared with Fig. 3.c - with short range interaction U_1 at $\theta=0.5$ - the stripes are a bit thicker, slightly less coherent and their distance is about one lattice constant larger.

3.5. Influence of short range interactions, the U_3 example

Variant 3 $U_3(s, \phi)$, Eq. (2.4) is more attractive and therefore strongly promotes adatoms to nucleate at next neighbor sites. We note in the pair distributions black dots at 1 lattice spacing in the $\langle 1-10 \rangle$ direction reflecting strong population of next neighbor sites.

Fig.5.a shows a sample configuration with short range interaction $U_3(s, \phi)$, Eq. (2.4) at coverage $\theta=0.1$. The cluster structure consists of a variety of sizes from monomers to n-mers. Fig.5.b shows the equivalent pair distribution taken from a configuration average. A reduced alignment of clusters to the substrate crystal directions is visible compared to Figs.3.b and 4.b.

Fig.5.c shows a sample configuration with short range interaction $U_3(s, \phi)$, Eq. (2.4) at coverage $\theta=0.3$. The cluster structure consists of larger islands some of which have merged to elongated islands with dog-bone-like shapes. Fig.5.d shows the equivalent pair distribution taken from a configuration average. The blue dots pretend an isotropic ring with a characteristic distance of 6, the g_{ik}

values of 1.1 at $s_{\langle 1-10 \rangle} = 5$ to 6 and of 1.3 at $s_{\langle 1-21 \rangle} = 3\sqrt{3}$, however, indicate a weak island alignment towards $\langle 1-21 \rangle$.

Fig.5.e shows a sample configuration with short range interaction $U_3(s, \phi)$, Eq. (2.4) at coverage $\theta=0.5$. The islands of lower coverages have merged to an interwoven stripe structure with an average stripe broadness of more than 3. Fig.5.f shows the equivalent pair distribution taken from a configuration average. Within the range of blue dots g_{ik} values of 1.05 at $s_{\langle 1-10 \rangle} = 5$ to 6 and of 1.1 at $s_{\langle 1-21 \rangle} = 3\sqrt{3}$ indicate very weak alignment towards $\langle 1-21 \rangle$. The characteristic distance is between 5 and 6. Compared with Fig. 4.e - with short range interaction U_2 at $\theta=0.5$ - the stripes look similar, but if Fig.5.f is compared with Fig.4.f we note a tendency towards a reduced order.

In summary the variants with more attractive short range interactions lead to less ordered superlattices consisting of more adatoms with a greater superlattice constant and thicker, more coherent stripes.

4. Discussion

In this section the model assumptions are reviewed, the model results are summarized and compared with experiments. The section closes with a discussion of open points.

4.1. Model assumptions

Assumptions and approximations used for this model have been discussed in [4] in detail. The most relevant approximation is an elastic continuum model for the substrates instead of a lattice model, known to be inadequate for describing short range effects. The elastic continuum model predicts a s^{-3} repulsion on the long range, a repulsive wall near 2.3 lattice distances and a strong attractive well at next neighbor distances.

The assumption of a perfectly flat surface excludes the effects of steps, known for their active role in nucleation and growth, partly due to strain in their neighborhood.

A further key assumption is thermal equilibrium for the adatom configurations, i.e. neglecting of kinetic effects.

Anisotropic stress generated by stretching adatom bonds is not covered.

Further assumptions cover the short range interactions used. Replacement of the deep attractive potential well by either a cap of about 5 units (in fact describing a strong repulsion of next neighboring adatoms) or by a cap at potential zero (in fact describing a weak repulsion of next neighboring adatoms) or by a cap at potential -5 units (describing a stronger attraction of next neighbors) is a method to indicate the effects of short range interactions while preserving the merits of a theory with medium range focus.

4.2. Comparison with previous off-grid simulations

The adatom configurations with interaction U_1 at $\theta=0.045$ resulting from an off-grid algorithm in [4] could be repeated with an on-grid algorithm. Both results and the derived pair distributions are consistent with the solution of a Born-Green-Ivon type integral equation describing the adatom pair distribution from Statistical Mechanics principles [7]. So the present simulations can be rated as a high coverage extension of previous results.

4.3. Adatom distribution on Cu $\langle 111 \rangle$

The results of sections 3.1 to 3.3 draw the picture of a substrate aligned hexagonal packed superlattice of adatoms or clusters at coverages up to $\theta \approx 0.3$ ML and stripes around coverages $\theta=0.5$ ML. The simulations predict a populated/unpopulated symmetry $\theta/(1-\theta)$. This is explained by minimization of the total configuration energy by forming adatom clusters or stripes or vacancies around 5 lattice distances apart. Substrate strain generated by adatoms stressing the surface is allowed to release within the unpopulated sites.

4.4. The role of short range interactions

The results of sections 3.4 and 3.5 indicate a strong role of short range interactions. The trends when increasing the short range attraction are

- larger clusters
- triangular instead of linear clusters (reflected by an increasing next neighbor pair distribution)
- more connected clusters
- less influence of the substrate on the superlattice and stripe directions, i.e. more isotropic configurations
- slightly increased feature size.

4.5. Comparison with experiments

Strain mediated superlattices on Cu $\langle 111 \rangle$ in the coverage region up to $\theta=0.045$ ML were already discussed and compared with experiments [10,11] in [4]. The agreement was good enough to propose strain mediated interactions as an alternative to the one discussed in [10,11]. The current investigation was triggered by an unknown referee of [4]. He raised the point how other manifestations of elastic interactions on surfaces, especially stress domains [12], are related to adatom superstructures.

Stress domains are ordered patterns of less dense and more dense adatom areas, for example adatom gas areas and monolayer areas forming spontaneously. They minimize surface energy by balancing short-range attractive with long-range repulsive interaction. Substrate strain created by surface stress in the more dense areas is allowed to relax in the less dense areas. The domains reflect the elastic anisotropy of the substrate.

- Observations at the Pb/Cu<111> system [5] can be characterized by
- ordered but mobile circular droplets (containing thousands of adatoms) at low coverages
 - stripes at medium coverage with a long range order improving when reducing temperature
 - ordered inverse droplets at high coverages approaching a monolayer (as predicted earlier, see references in [5]).

The periodicity of patterns is in the 100 nm range, decreasing with increasing temperature. The observed temperature range is 623 K to 673 K. The order of droplets can - from a first glance - be interpreted as a superlattice type.

The sequence of island superlattices, domain patterns and inverse droplets on Pb/Cu<111> with increasing coverage observed in [5] would serve as a striking experimental evidence of the theory and the simulation results presented in section 3.4 if the length scales and the temperature would be the same. Unfortunately [5] describes a high temperature experiment with adatom clusters of thousands of adatoms while the experiments showing superlattice effects on a few lattice constant scale have been performed in the 10K region [10,11]. So the question arises if the present Molecular Dynamics simulation could be extended to handle clusters and structures of hundreds or thousands of adatoms. Unfortunately this would be far beyond the resources of a PC, so we must rely on scaling arguments to argue the same driver - elastic interactions - for both phenomena, adatom superlattices and stress domain patterns:

Following the cluster section of [8] we argue a simple superposition ansatz for the elastic interactions: two clusters of n_1 and n_2 adatoms create n_1*n_2 times the elastic inter cluster energy of two single adatoms. This ansatz, of course, is a strong restriction not considering e.g. short range adatom-adatom interactions and lattice mismatch effects.

Two $n=10^3$ clusters would create an interaction U^{Cluster} 10^6 times U . The temperature range for the stress domain experiments at 650 K is a factor 10^2 higher than the regime of single adatom effects, so the scaled cluster interaction $u^{\text{Cluster}}=U^{\text{Cluster}}/k_B T$ would be 10^4 times higher. The typical length s^{Cluster} according to Eq. (2.9) would then be $10^{4/3} \approx 21$ times higher than s . The coverage θ^{Cluster} would be reduced by a factor of about 464 (noting that the coverage of adatoms and of clusters have different meaning).

We summarize that length scales may differ from 5 substrate lattice constants to 100 lattice constants in the example above, but the elastic interaction mechanism is the same.

It would be a big surprise if such simple scaling arguments could explain the physics of stress domains more than qualitatively. In fact the measurement in [15] shows a decrease in domain feature size from 140 nm to 40 nm when the temperature rises from 590 K to 650 K, far beyond the above scaling effects. The authors explain such decrease in stripe periodicity with the change in domain-boundary free energy caused by thermally broken Pb-Pb bonds. Thus the effects of short range interactions override the effects of elastic medium range interactions under certain conditions. This is not in contradiction to the scaling arguments above since Eq. (2.9) is valid only for a s^{-3} type interaction which

does not include short range effects.

The influence of substrate anisotropy as observed in [13] is reflected in the present simulations and the pair distributions derived. The dominating stripe orientation at coverage $\theta=0.5$ ML reported is $\langle -1-12 \rangle$, the model results show a weak stripe orientation in the same directions.

The assumed equilibrium conditions are confirmed by experiments with reversible shape transitions (droplet to elongated islands with dog-bone-like shapes) during heating cycles [14]. An increase in temperature changes the shapes the same way as an increasing coverage does, again in line with the scaling arguments outlined above (same shape of $g(s, u_0, \theta)$ if u_0 reduced or θ increased). Both experimental results can be seen as a hint for the validity of the assumptions and conclusions.

The lack of details reported makes the comparison of further experiments with the present model similarly difficult. Two further examples should show its ability and its limitations:

N on Cu $\langle 111 \rangle$ forms elongated islands, stable at room temperature, aligned in 3 equivalent crystal directions. The islands show a characteristic distance of about 10 nm and are often colliding [16]. Since coverage and crystal directions are not reported, a comparison with stripes as calculated from the model is incomplete, but similarities with Figs. 3.e, 4.e, 5.e should encourage further research.

Co on Cu $\langle 111 \rangle$ acts as a nanoisland reference system with a well documented strain mediated morphologies [17, 18]. They are different from the ones found in this calculations due to their tendency of bi-layer growth even at moderate coverages. Triangular bi-layer islands show lateral displacements of the Co-Co bond lengths (measured by the surface state electron energy) dependent on their positions within the islands, associated with lateral strain.

The following picture for strain mediated morphologies is concluded: Stripe morphologies correlate with repulsive short range interaction while attractive short range interactions destabilize stripes and - via multilayer growth - lead to islands. Islands create strain and interact via strain and their shape minimizes elastic energy.

4.6. Open questions

Clusters arranged in superlattices and stress domain patterns on Cu $\langle 111 \rangle$ in the temperature range of about 10K with a characteristic length of about 5 to 6 lattice constants hopefully may be found in existing material. More experimental material is needed to determine size and nature of short range interactions and also the orientation of cluster/ stripe structures relative to the substrate crystal directions.

First principles methods (like density-functional-theory) need to be applied for estimating the stress parameters.

A further question is how the theory successfully describing mesoscopic stress patterns [12] can be utilized to better understand the microscopic effects discussed in the present analysis: When domain boundary effects play an impor-

tant role in the mesoscopic range, the effects of short range interactions in the microscopic range should be similarly significant.

The morphology of adatoms on other surfaces is an equally interesting topic, the much stronger effects of elastic anisotropy on $\langle 001 \rangle$ surfaces of many materials is expected to lead to further insight. Increasing the accuracy of the simulation by increasing the diameter of the simulation area on much more powerful computers may also lead to additional insights.

Bi-layer effects would extend the scope of the model but require some basic work. It should be noted that long range magnetic interactions should also be considered in the Co case.

The restrictions of the present isotropic stress model motivated an extension of the model [19]: Dimers are supposed to create anisotropic stress by stretching their bond. Such stress creates other types of elastic interactions including lattice mismatch.

7. Summary

Substrate strain mediated adatom configurations have been simulated for $\text{Cu}\langle 111 \rangle$ surfaces for three short range interaction types. The adatom coverages range up to nearly a monolayer. Pair distributions have been derived to prove morphologies from superlattices of single adatoms and clusters to ordered stress domain patterns. Higher coverages beyond 0.5 monolayers show vacancy structures just inverted. The short range interaction shows a significant influence on the cluster size within the superlattices. Substrate elastic anisotropy influences the superlattice orientation with respect to the substrate crystal directions.

Experiments showing similar structures have been compared with the model. For low temperatures superlattices of single adatoms have been found while for increased temperatures ordered islands and stripes of adatoms have been reported. There is some evidence of elastic interactions being the common cause but a final conclusion on the validity of the theory remains open at this point in time.

Erratum

In the course of recent calculations a code fault affecting previous results [4,7] was detected: The $\cos(p\pi/2)$ term in Eq. (2.1) was omitted in the code there. Therefore the $p=6$ interaction terms on $\langle 111 \rangle$ surfaces had a sign error. As a consequence the results have to be rotated by 30° . In the current version of this paper the fault has been corrected. The author apologizes for any inconvenience.

References

- [1] H.Brune, Creating Metal Nanostructures at Metal Surfaces Using Growth Kinetics, in: Handbook of Surface Science Vol.3 (E.Hasselbrink and B.I.Lundqvist ed.), Elsevier, Amsterdam (2008)
- [2] H.Ibach, Surf.Sci.Rep. 29, 195 (1997)
- [3] T.L.Einstein, Interactions between Adsorbate Particles, in: Physical Structure of Solid Surfaces (W.N.Unertl ed.), Elsevier, Amsterdam (1996)
- [4] W.Kappus, Surf. Sci. 609, 30 (2013)
- [5] R.Plass, J.A.Last, N.C.Bartelt, G.L.Kellogg, Nature 412, 875 (2001)
- [6] L.Proville, Phys. Rev. B 64, 165406 (2001)
- [7] W.Kappus, Surf. Sci. 606, 1842 (2012)
- [8] W.Kappus, Z.Physik B 29, 239 (1978)
- [9] A.G.Every, A.K.McCurdy: Table 3. Cubic system. Elements. D.F.Nelson(ed.), SpringerMaterials- The Landolt-Börnstein Database
- [10] J.Repp, F.Moresco, G.Meyer, K.H.Rieder, P.Hyldgaard and M.Persson, Phys. Rev. Lett. 85, 2981 (2000).
- [11] F.Silly, M.Pivetta, M.Ternes, F.Patthey, J.P.Pelz, W.D.Schneider, New J. of Phys. 6, 16 (2004)
- [12] O.L.Alerhand, D.Vanderbilt, R.D.Meade, J.D.Joannopoulos, Phys. Rev. Lett. 61, 1973 (1988)
- [13] F.Leonard, N.C.Bartelt, G.L.Kellogg, Phys. Rev. B 71, 045416 (2005)
- [14] R.van Gastel, N.C.Bartelt, G.L.Kellogg, Phys. Rev. Lett. 96, 036106 (2006)
- [15] R.van Gastel, N.C.Bartelt, P.J.Feibelman, F.Léonard, and G.L.Kellogg, Phys. Rev. B 70, 245413 (2004)
- [16] F.M.Leibisler, Surf. Sci. 514, 33 (2002)
- [17] M.V.Rastei, B.Heinrich, L.Limot, P.A.Ignatiev, V.S.Stepanyuk, P. Bruno, J.P.Bucher, Phys. Rev. Lett. 99, 246102 (2007)
- [18] N.N.Negulyaev, V.S.Stepanyuk, P. Bruno, L.Diekhöner, P.Wahl, K.Kern, Phys. Rev. B 77, 125437 (2008)
- [19] W.Kappus, <http://arxiv.org/abs/1301.3643>

Acknowledgement

Many thanks to the unknown referee of [4] for directing the author's interest to stripes.

Appendix

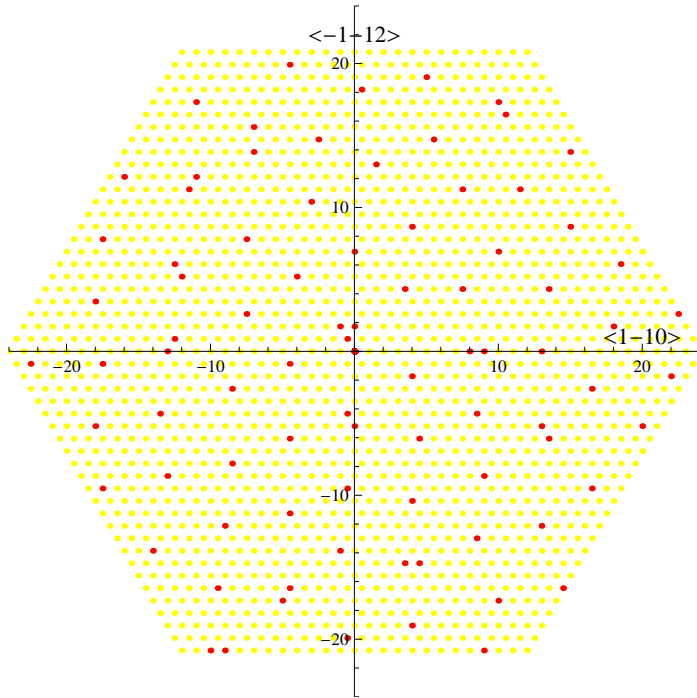


Fig. 1.a shows a sample configuration with reference short range interaction $U_1(s, \phi)$ (2.2) and a coverage $\theta=0.045$.

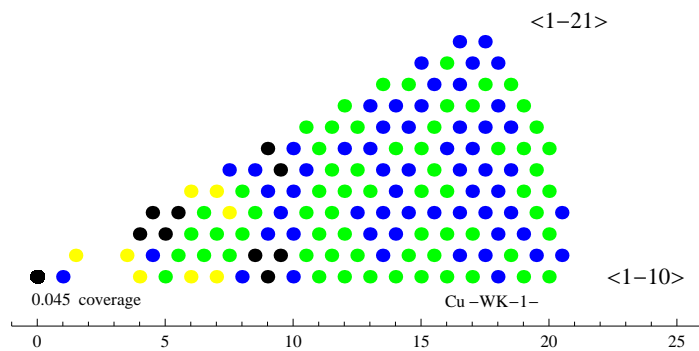


Fig. 1.b shows an average adatom pair distribution in a 30 degree sector with reference short range interaction $U_1(s, \phi)$ (2.2) and a coverage $\theta=0.045$. The differently colored dots represent different values of the pair distribution (darker colors represent higher values).

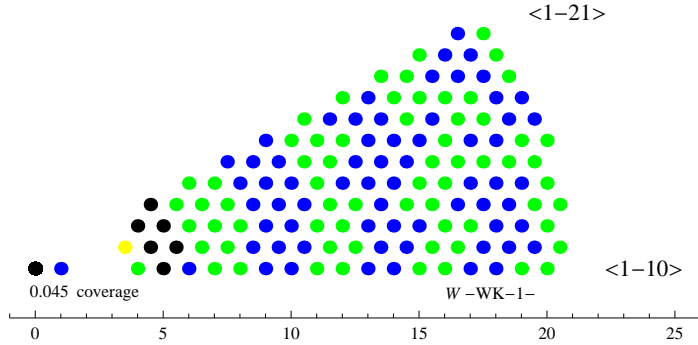


Fig.2 shows an average pair distribution for an isotropic substrate (tungsten) at coverage $\theta=0.045$ in a 30 degree sector.

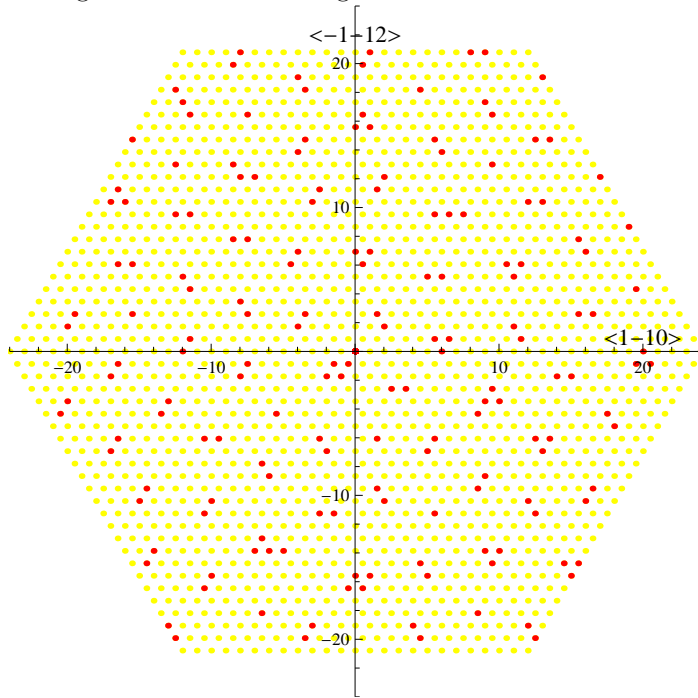


Fig.3.a shows a sample configuration with short range interaction $U_1(s, \phi)$ (2.2) at coverage $\theta=0.1$.

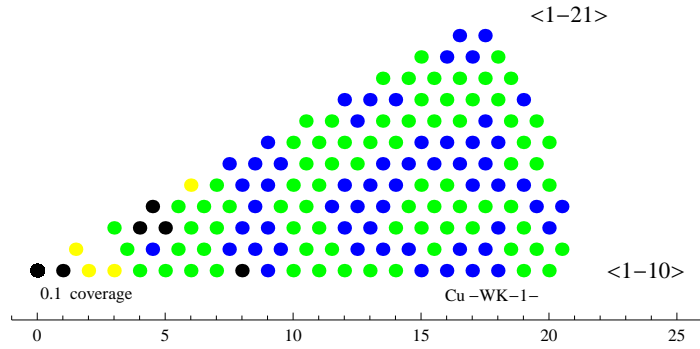


Fig.3.b shows an average pair distribution with short range interaction $U_1(s, \phi)$ (2.2) at coverage $\theta=0.1$.

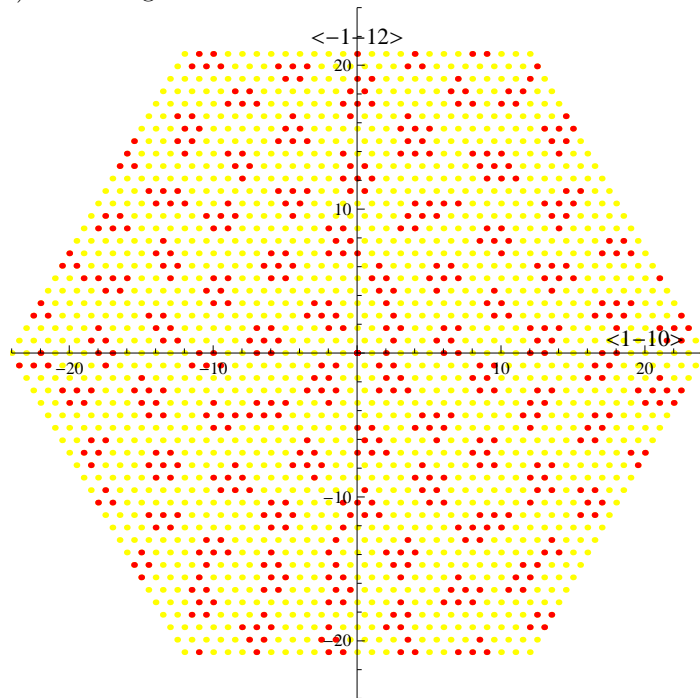


Fig.3.c shows a sample configuration with short range interaction $U_1(s, \phi)$ (2.2) at coverage $\theta=0.3$.

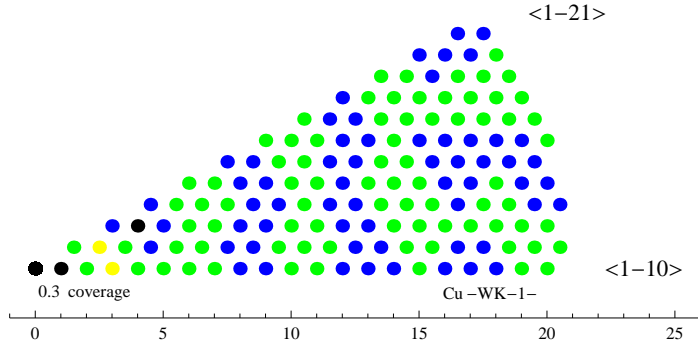


Fig.3.d shows an average pair distribution with short range interaction $U_1(s, \phi)$ (2.2) at coverage $\theta=0.3$.

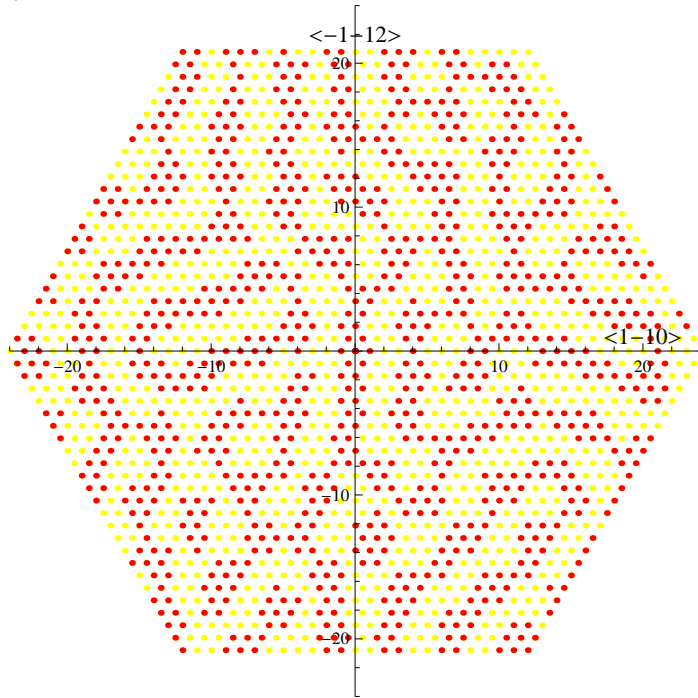


Fig.3.e shows a sample configuration with short range interaction $U_1(s, \phi)$ (2.2) at coverage $\theta=0.5$.

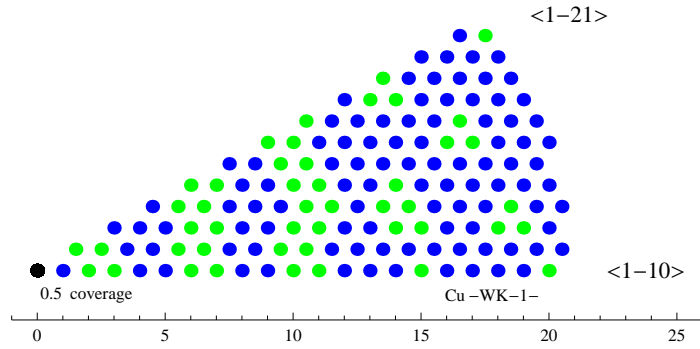


Fig.3.f shows an average pair distribution with short range interaction $U_1(s, \phi)$ (2.2) at coverage $\theta=0.5$.

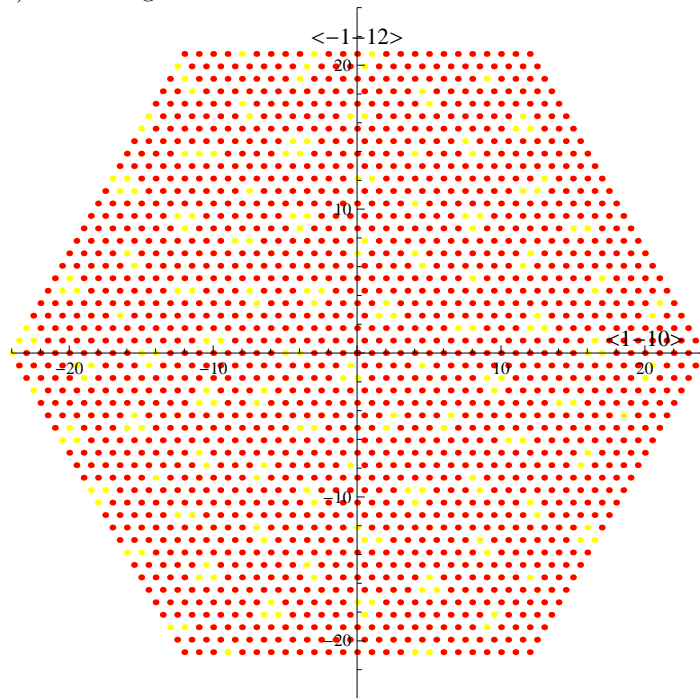


Fig.3.g shows a sample configuration with short range interaction $U_1(s, \phi)$ (2.2) at coverage $\theta=0.9$.

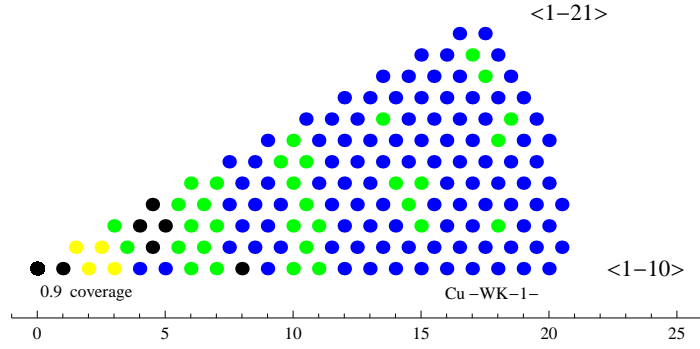


Fig.3.h shows an average vacancy pair distribution (3.1) with short range interaction $U_1(s, \phi)$ (2.2) at coverage $\theta=0.9$.

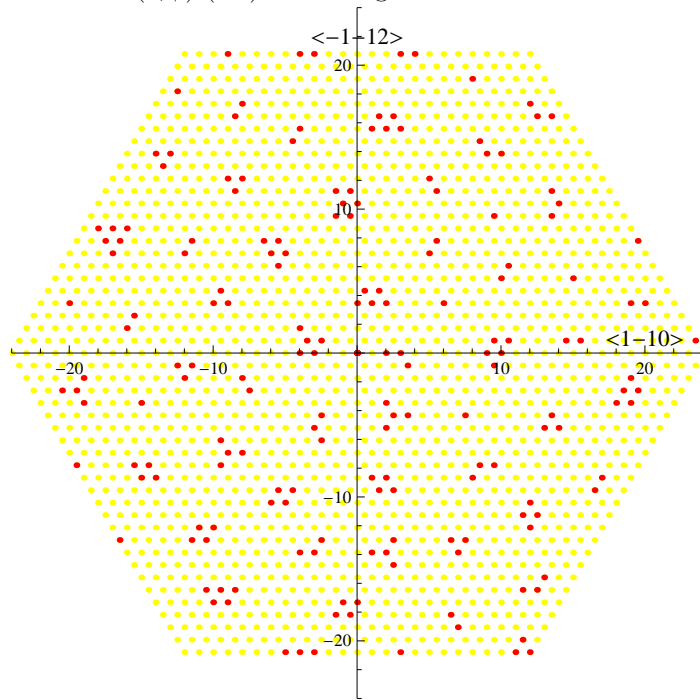


Fig.4.a shows a sample configuration with short range interaction $U_2(s, \phi)$ (2.3) at coverage $\theta=0.1$.

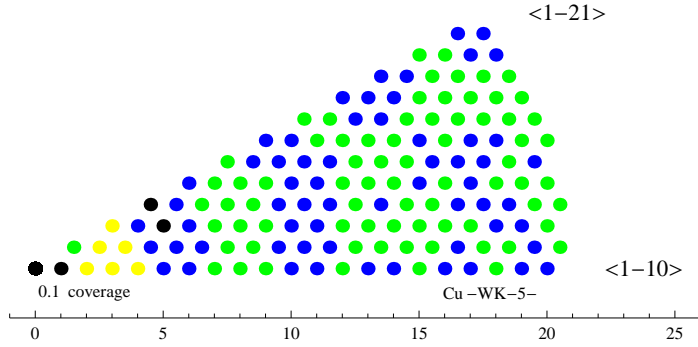


Fig.4.b shows an average pair distribution with short range interaction $U_2(s, \phi)$ (2.3) at coverage $\theta=0.1$.

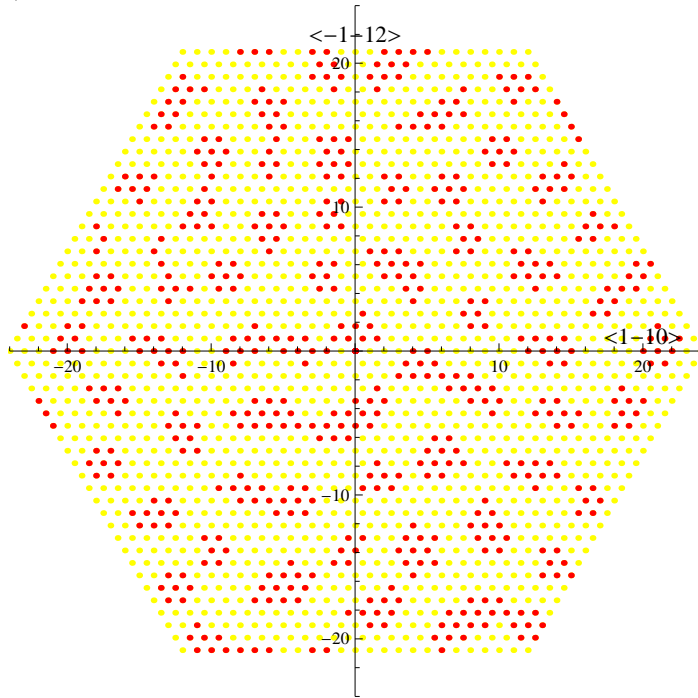


Fig.4.c shows a sample configuration with short range interaction $U_2(s, \phi)$ (2.3) at coverage $\theta=0.3$.

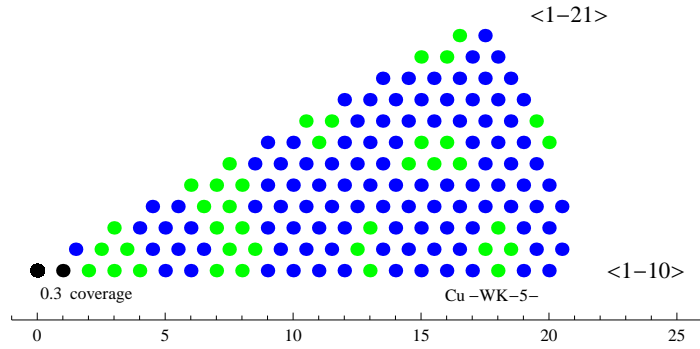


Fig.4.d shows an average pair distribution with short range interaction $U_2(s, \phi)$ (2.3) at coverage $\theta=0.3$.

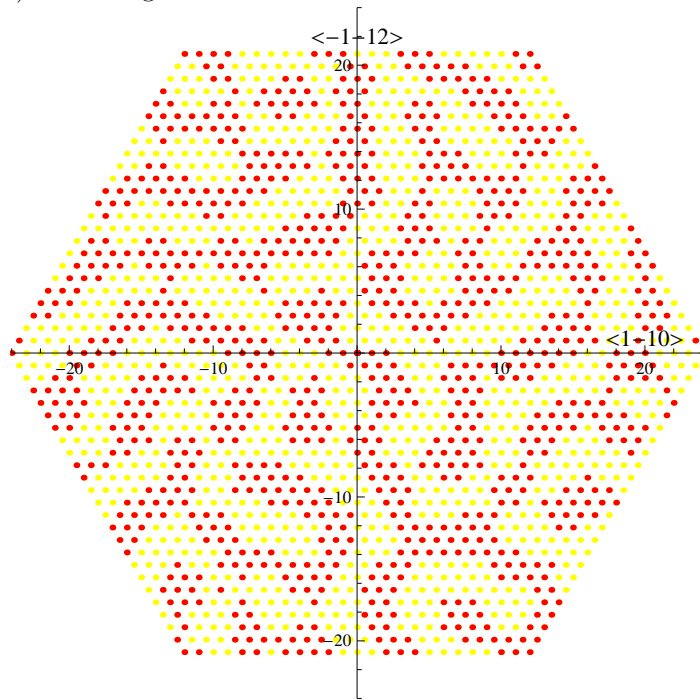


Fig.4.e shows a sample configuration with short range interaction $U_2(s, \phi)$ (2.3) at coverage $\theta=0.5$.

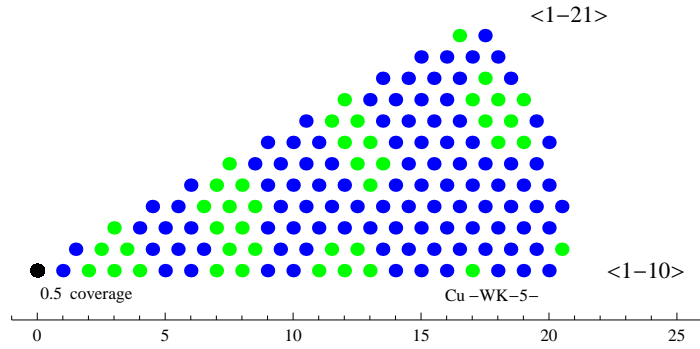


Fig.4.f shows an average pair distribution with short range interaction $U_2(s, \phi)$ (2.3) at coverage $\theta=0.5$.

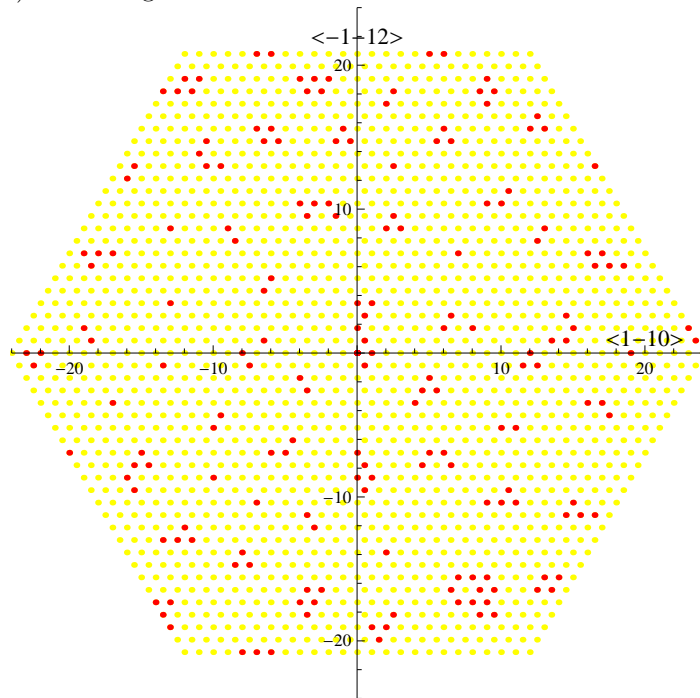


Fig.5.a shows a sample configuration with short range interaction $U_3(s, \phi)$ (2.3) at coverage $\theta=0.1$.

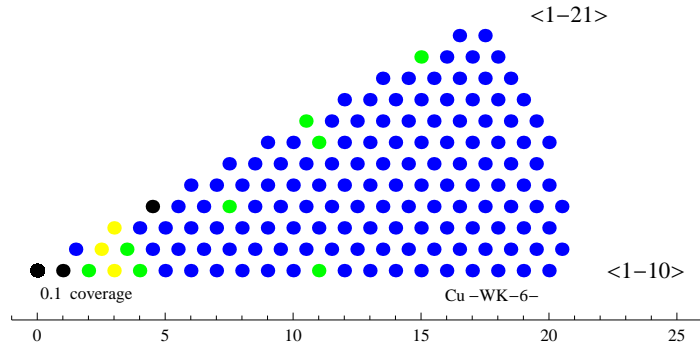


Fig.5.b shows an average pair distribution with short range interaction $U_3(s, \phi)$ (2.3) at coverage $\theta=0.1$.

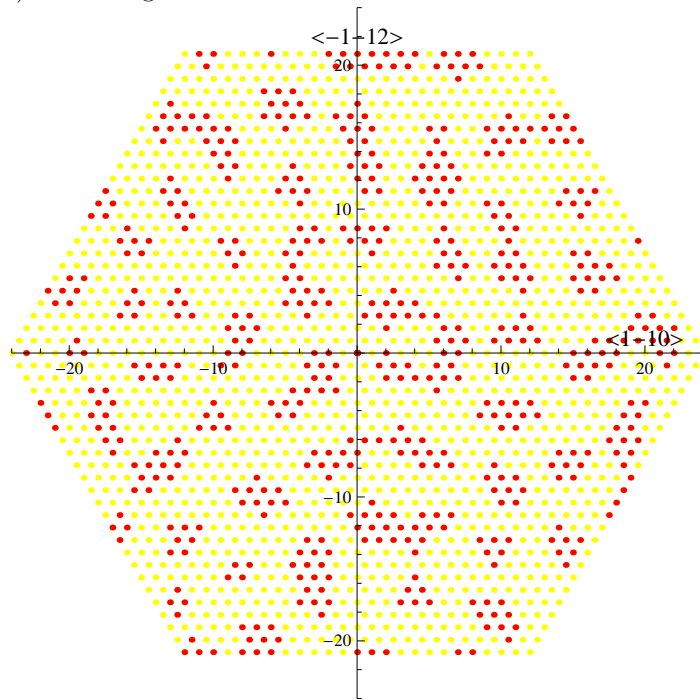


Fig.5.c shows a sample configuration with short range interaction $U_3(s, \phi)$ (2.3) at coverage $\theta=0.3$.

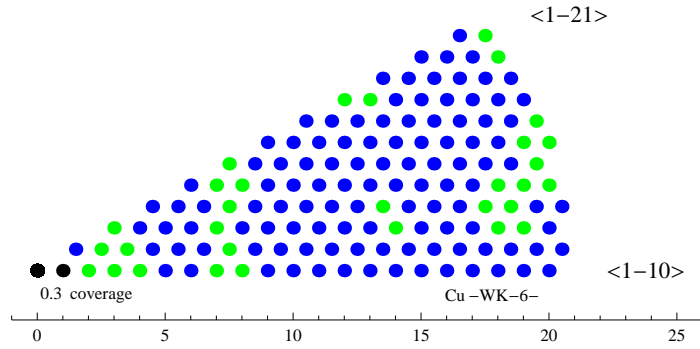


Fig.5.d shows an average pair distribution with short range interaction $U_3(s, \phi)$ (2.3) at coverage $\theta=0.3$.

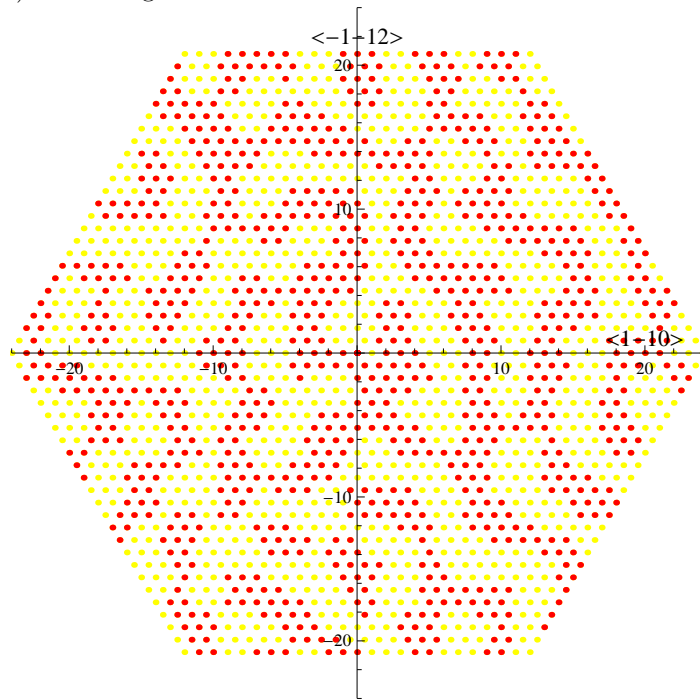


Fig.5.e shows a sample configuration with short range interaction $U_3(s, \phi)$ (2.3) at coverage $\theta=0.5$.

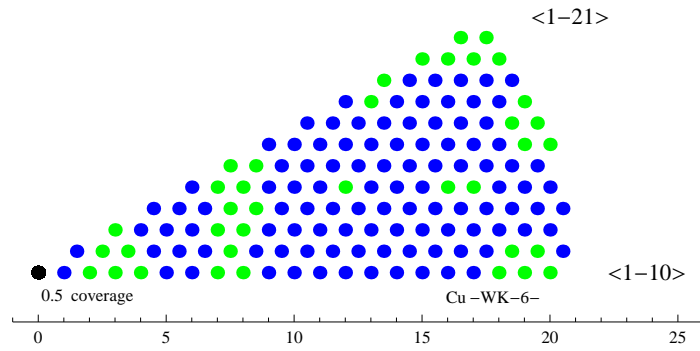


Fig.5.f shows an average pair distribution with short range interaction $U_3(s, \phi)$ (2.3) at coverage $\theta=0.5$.

© Wolfgang Kappus 2012